Perturbation of Rb, p53 and Brca1 or Brca2 cooperate in inducing metastatic serous epithelial ovarian cancer

Ludmila Szabova[1,6], **Chaoying Yin**[2,6], **Sujata Bupp**[1], **Theresa M. Guerin**[1], **Jerome J. Schlomer**[1], **Deborah B. Householder**[1], **Maureen L. Baran**[1], **Ming Yi**[3], **Yurong Song**[2,5], **Wenping Sun**[3], **Jonathan E. McDunn**[4], **Philip L. Martin**[1], **Terry Van Dyke**[1,2,5], and **Simone Difilippantonio**[1,*]

[1]Center for Advanced Preclinical Research, SAIC at Frederick National Laboratory for Cancer Research (FNLCR), MD 21702, USA

[2]Department of Genetics, University of North Carolina at Chapel Hill, Chapel Hill, NC 27599, USA

[3]Advanced Biomedical Computing Center, SAIC at Frederick National Laboratory for Cancer Research (FNLCR), MD 21702, USA

[4]Metabolon, Incorporated, Durham, NC, 27713, USA

[5]Mouse Cancer Genetics Program Frederick National Laboratory for Cancer Research (FNLCR), MD 21702, USA

Abstract

The majority of human high grade serous epithelial ovarian cancer (SEOC) is characterized by frequent mutations in p53 and alterations in the RB and FOXM1 pathways. A subset of human SEOC harbors a combination of germline and somatic mutations as well as epigenetic dysfunction for BRCA1/2. Using Cre-conditional alleles and intrabursal induction by Cre-expressing adenovirus in genetically engineered mice, we analyzed the roles of pathway perturbations in epithelial ovarian cancer initiation and progression. Inactivation of RB-mediated tumor suppression induced surface epithelial proliferation with progression to stage I carcinoma. Additional biallelic inactivation and/or missense p53 mutation in the presence or absence of Brca1/2 caused progression to stage IV disease. As in human SEOC, mice developed peritoneal carcinomatosis, ascites, and distant metastases. Unbiased gene expression and metabolomic profiling confirmed that Rb, p53, and Brca1/2-triple mutant tumors aligned with human SEOC, and not with other intraperitoneal cancers. Together, our findings provide a novel resource for evaluating disease etiology and biomarkers, therapeutic evaluation, and improved imaging strategies in epithelial ovarian cancer.

Keywords

Ovarian cancer; GEM model; p53; Brca; Rb

*Corresponding author: Simone Difilippantonio, 1050 Boyles Street, Building 539, Room 229, Frederick, Maryland 21702, phone: (301) 228-4465, fax: (301) 846-6666, difilips@mail.nih.gov.
[6]these authors contributed equally

Introduction

Ovarian cancer is the 5th deadliest disease among American women (1), with over 50% presenting with serous papillary histology. High grade serous epithelial ovarian cancer (SEOC) is associated with intraperitoneal spreading (carcinomatosis) and distant metastases. Standard treatment is aggressive surgical resection followed by platinumtaxane chemotherapy. Platinum-resistant cancer recurs in approximately 25% of patients within 6 months (2), and the overall five-year survival probability is 31% (3). Current methods for early detection, such as transvaginal ultrasound and blood Cancer Antigen 125 (CA125) levels have shown limited effectiveness (4, 5).

The Cancer Genome Atlas (TCGA) study of a large high grade SEOC cohort revealed that mutations in TP53 predominated, occurring in at least 96% of tumors (6). Brca1 and Brca2 were mutated in 22% of tumors, representing a combination of germline and somatic mutations (6). Known cancer-associated pathways such as RB1 and PI3K/RAS were deregulated in 67% and 45% of cases, respectively (6).

Advances in modeling cancers in genetically engineered mice (GEM) have facilitated mechanistic understanding of tumor development and applicability in preclinical studies for several cancers [reviewed in (7-9)]. GEM models of endometrioid (10) and other epithelial ovarian cancers (11-15) have been generated based on alterations of specific genetic pathways. While two studies showed that concomitant inactivation of Brca1 and p53 or Rb1 and p53 in mouse ovarian surface epithelium (OSE) cells can give rise to carcinomas with serous histology, respectively (11, 16), in two other studies ovary-specific conditional inactivation of Brca1 and p53, in the presence or absence of Rb, resulted in ovarian leiomyosarcomas (13, 15). Despite these extensive studies, the combination of pathway perturbations leading to consistent initiation and progression of metastatic SEOC-like disease in the mouse has been elusive. Here, we describe a comprehensive temporal study of the most common pathways altered in human SEOC. Using selective induction of individual or combinations of *Brca1 or Brca2, p53* knockout and/or mutant alleles and Rb tumor suppression (Rb-TS) inactivation, we analyzed the relative contribution to disease progression from tumor initiation to invasive carcinomas with carcinomatosis and distant metastases. Genome-wide expression, serum metabolomic and marker studies indicate that perturbing all three pathways yields disease arising from OSE with the characteristics of human SEOC.

Materials and Methods

Experimental animals

All experimental animals were maintained in accordance with the Institutional Animal Care and Use Committee (ACUC) and the NIH Guide for the Care and Use of Laboratory Animals. All procedures performed on mice were approved by the ACUC of Frederick National Laboratory for Cancer Research (FNLCR), Maryland. *Brca1$^{fl/fl}$* [FVB;129-*Brca1^{tm2Brn}*], *Brca2$^{fl/fl}$* [STOCK *Brca2^{tm1Brn}*], *p53$^{fl/fl}$* [FVB;129-*Trp53^{tm1Brn}*] and *p53^{LSL} R172H/+* [129S4-*p53^{tm2Tyj}*] mice were obtained from the MMHCC Mouse Repository (National Cancer Institute, Rockville, MD, USA). Conditional *TgK18GT$_{121}$$^{tg/+}$* BAC transgenic mice were generated by insertion of a floxed eGFP STOP T$_{121}$ cassette several base pairs upstream of the 1st ATG start codon in exon 1 of the Keratin 18 gene by recombineering (17). *Rosa26STOPfloxLacZ* reporter mice [B6;129-*Gt(ROSA)26SorT^{M1sor}*] were purchased from the Jackson Laboratory.

Adenovirus administration

Recombinant adenovirus Ad5-CMV-Cre (Adeno-Cre) was purchased from the University of Iowa Transfer Vector Core at a titre of 10^{11}-10^{12} infectious particles/ml. To demonstrate our capability to successfully perform intrabursal inductions, we performed intrabursal injections of Adeno-Cre as previously described (11) on 7-8 week-old female *ROSA26STOP^{floxP}lacZ* reporter mice. The right ovary was injected with approximately 7 µL of Adeno-Cre virus into the ovarian bursa near the oviducts during survival surgery 36 hours following super ovulation. Injected *ROSA26STOP^{floxP}lacZ* females were euthanized 2 weeks post injection, ovaries were removed and whole mounts stained for LacZ expression (Supplementary Material and Methods).

Tissue collection, pathological and immunohistochemical analysis

Animals were euthanized by CO_2 inhalation, ovaries and other affected organs were fixed in 10% neutral buffered formalin, processed for paraffin embedding and characterized by microscopic evaluation. Five µm serial sections were cut for H&E and IHC. Pathological evaluation of histological findings was performed by a board certified veterinary pathologist (P. L. M.) according to existing human epithelial ovarian cancer classifications [International Federation of Gynecology and Obstetrics (FIGO)].

Paraffin sections were deparaffinized in xylene, rehydrated in ethanol according to standard protocol and subsequently used for IHC stains. Antibodies and conditions used for IHC stains are listed in Supplementary Material and Methods. For all IHC stains 3,3′-Diaminobenzidine (DAB) (Sigma) substrate was used to visualize peroxidase activity followed by hematoxylin counterstain, dehydration and mounting.

Detailed procedures and primer sequences used for genotyping and detection of recombined alleles, LacZ staining, MR imaging, microdissection and sequencing, metabolome profiling and gene expression profiling can be found in Supplementary Materials and Methods.

Results

Conditional inactivation of RB tumor suppression in OSE causes stage I SEOC

Based on the frequency with which Rb is altered in human cancers, redundancy among the pRb family proteins appears to be more widespread in the mouse than in the human. Indeed, recent cancer genome studies indicate that several points in this pathway are altered, but in a mutually exclusive pattern for individual tumors. The sum of these lesions indicates that most human solid malignancies, including SEOC, are aberrant in RB-TS (18). Given the limitation of allele combinations possible in the GEM experimental systems and the redundancy in the pathway, we used an epithelial-specific Cre-dependent allele expressing T_{121} to dominantly interfere with all three pocket proteins (pRB, p107 and p130), thus facilitating RB-TS inactivation in vivo with a single allele (19, 20). T_{121} (the N-terminal domain of SV40 T antigen) was directed to OSE using transgenic *TgK18GT$_{121}$* mice that carry a bacterial artificial chromosome (BAC) containing the mouse cytokeratin (CK) 18 gene, into which a Cre-conditional loxP-GFP-stop-loxP (LSL) T_{121} cassette was inserted (Fig. 1A) (17). To selectively induce T_{121} in OSE, adenoviral Cre (Adeno-Cre) was introduced under the bursa (Suppl. Figure S1A a,b). Deletion efficiency was monitored by IHC 3 months post induction (pi) for GFP (no deletion), T_{121} (deletion) and CK18 (cell type) (Fig. 1A, B). GFP was detected diffusely in CK18 expressing OSE cells of the uninjected and in some cells of the injected ovary (Fig. 1B a,b). T_{121} was present only in OSE cells of the injected ovary (Fig. 1B c,d), indicating successful recombination within the *TgK18GT$_{121}$* transgene. Mice were examined at various times pi. All uninjected ovaries were normal up to 24 months pi (Fig. 1 B a,c,e). In contrast, 72 % (16/22) of injected

$TgK18GT_{121}$ ovaries had cytologic abonormalities in the OSE. Of these, 27% (6/22) developed minimal to mild atypical hyperplasia with occasional papillary epithelial projections 3 to 24 months pi. An additional 27% (6/22) of mice had OSE carcinoma in situ (CIS) with no significant invasion into the underlying ovary or overlying bursa (5 and 24 months pi, Fig. 1C a,b, Fig. 2A). In 18% (4/22) of induced $TgK18GT_{121}$ mice, the ovarian tumors had progressed to SEOC pathology with early invasion into ovary and bursa (Fig. 1Cc,d; 2A). Histologically, tumors were characterized by high mitotic (>12 mitoses per ten 40× fields) and apoptotic rates (Fig. 1C c,d), consistent with the acute induction of these outcomes in other cell types upon RB-TS inactivation (21). In summary, inactivation of RB-TS was sufficient to cause OSE proliferation, with progression only to stage I disease (WT vs $TgK18GT_{121}$, Man Whitney test, p<0.0001).

Brca1/2 or p53 mutations/deletions alone or in combination fail to initiate OSE pathology

The current report of high frequency of TP53 mutations and involvement of Brca1 and Brca2 aberrations in human SEOC patients (6) prompted us to examine roles for these perturbations in mouse SEOC. Since p53 missense mutations have tissue and mutant-specific functions that can differ from loss of protein (22),(23), we evaluated both conditional inactivation ($p53^{fl/fl}$) and missense mutation $p53^{R172H}$ expression using the Adeno-Cre induction described above. The p53 DNA binding mutation R172H is analogous to the R175H hotspot mutation frequently identified in human cancers, including ovarian carcinomas (24). In addition, we generated mice with allele combinations in order to model the frequent loss of the remaining wild-type $p53$ allele observed in human tumors.

Reproductive tracts and affected organs of all single and double combinations of Brca1, Brca2 and p53 alleles were analyzed (Brca1$^{fl/fl}$, Brca2$^{fl/fl}$, p53$^{R172H/+}$, p53$^{fl/fl}$, p53$^{R172H/fl}$, Brca1$^{fl/fl}$/p53$^{R172H/+}$, Brca1$^{fl/fl}$/p53$^{R172H/fl}$, Brca1$^{fl/fl}$/p53$^{fl/fl}$, Brca2$^{fl/fl}$/p53$^{R172H/+}$, Brca2$^{fl/fl}$/p53$^{R172H/fl}$, Brca2$^{fl/fl}$/p53$^{fl/fl}$). None of the injected or un-injected ovaries from these mice displayed pathological changes in the OSE up to 24 months pi (Figure 2B, Table 1). $Brca1^{fl/fl}$ and $Brca2^{fl/fl}$ mice developed non-ovarian neoplasms at a similar frequency as wildtype mice (Suppl. Table 1). However, mice carrying the $p53^{R172H}$ allele, a null allele before recombination, developed an increased frequency of lymphomas and sarcomas consistent with the tumor spectrum of $p53^{+/-}$ mice (25) (Suppl. Table 1). The failure to elicit OSE pathology alone or in combination indicates that perturbation of p53 and/or Brca1/2 cannot initiate and may instead progress disease.

Histopathological features of SEOC in Rb, p53 and Brca1/2 compound mice parallel human disease

To model the concurrent dysregulation of RB-TS and p53 with or without Brca1 or Brca2 pathways, we generated mice carrying a range of allele combinations. The frequency of SEOC pathology development among these animals varied as follows: 72% $TgK18GT_{121}{}^{tg/+}/p53^{R172H/fl}$, 88% $TgK18GT_{121}{}^{tg/+}/p53^{fl/fl}$, 70% $TgK18GT_{121}{}^{tg/+}/Brca1^{fl/fl}/p53^{R172H/fl}$, 68% $TgK18GT_{121}{}^{tg/+}/Brca2^{fl/fl}/p53^{R172H/fl}$ and 78% $TgK18GT_{121}{}^{tg/+}/Brca1^{fl/fl}/p53^{fl/fl}$ (Table 1, Fig. 2C-E). Disease progression in these mice was staged in a manner similar to the human ovarian carcinoma staging scheme (FIGO) (Fig. 2F, Suppl. Fig. S1B,C) (26).

Ovarian tumor development could be followed by MRI and resulted in large palpable masses on the injected ovary along with hemorrhagic or serous ascites (Fig. 3A-C). OSE carcinomas showed a range of morphological patterns observed in SEOC of women, including papillary, micropapillary/filigree, microcystic, poorly differentiated adenocarcinoma and solid/undifferentiated (Fig. 3D-I). Multiple histological patterns were frequently observed in the same tumor. The cytology was often high grade with prominent

cellular/nuclear pleomorphism and >10 mitoses per 40× field. Similar to SEOC in humans, the mice developed multifocal peritoneal carcinomatosis with tumor spread to all abdominal organs (Fig. 3J). Distant metastases were also observed, and followed a pattern similar to that reported in humans (27). Metastases were observed in the pleura of 87.5% (21/24) (Fig. 3K), in the lung of 83% (20/24) and in the liver of 46% (11/24) of mice with stage IV disease (Fig. 3L).

In addition to pathological changes in the OSE, 2% (11/537) of mice had transformation of the oviduct epithelium. The oviduct lesions ranged from atypical hyperplasia (4/11) to carcinoma in-situ (3/11) to adenocarcinoma (4/11). In contrast to the OSE lesions which primarily had a papillary morphology, the oviduct lesions were characterized by a glandular/acinar histology (Fig. 4). Based on these significant histological differences, it is considered unlikely that any of the carcinomatosis or metastasis arose from these oviduct adenocarcinomas.

Immunohistochemical analysis confirmed that all SEOC, peritoneal and distant metastases expressed T_{121} and CK18. Further immunophenotyping revealed expression of CA125 and Wilms' tumor 1 (WT1), markers typically expressed in human SEOC (28, 29), in OSE and carcinoma cells (Suppl. Fig. S2A). Pax8 and Calretinin staining (Suppl. Fig. 2B) has been used to differentiate between human SEOC (Calretinin−, Pax8+) and intraperitoneal mesothelioma (Calretinin+, Pax8−) (30, 31). While normal murine OSE and most SEOCs were Pax8 negative, 9% (2/22) SEOC and peritoneal carcinomatosis had rare (<1% of cells) Pax8 expression (Fig. 4). In contrast, all of the oviduct adenocarcinomas had strong nuclear Pax8 expression similar to the normal oviduct epithelium (Fig. 4a-f). To further distinguish SEOC from intraperitoneal malignancies, such as diffuse malignant peritoneal mesothelioma (DMPM), we determined the staining patterns for estrogen receptor (ER), progesterone receptor (PR) and cytokeratins CK5 or CK6. As in human SEOCs (30, 32-35), normal murine OSE and carcinoma cells as well as abdominal carcinomatosis and metastases were strongly ER positive with rare expression of PR and did not express CK5 or CK6 (Fig. 4g-x, Supplementary Material and Methods). In contrast, a human DMPM was CK5/CK6+, ER− and PR− as expected (Fig. 4 f, l, r, x) (33-35). In summary, these mice develop tumors that grossly, histologically and immunophenotypically resemble human SEOC.

Role of Brca1/2 and p53 in tumor progression

The overall penetrance of SEOC in compound mutants containing RB-TS, biallelic p53 with or without Brca1/2 deletion was very similar (Table 1, Fig. 2E). The inactivation of Brca1 increased the incidence of stage III and IV SEOC from 8% in $TgK18GT_{121}{}^{tg/+}/p53^{R172H/+}$ mice to 16% in $TgK18GT_{121}{}^{tg/+}/Brca1^{fl/fl}/p53^{R172H/+}$ mice (Table 1, Fig. 2E). However, this increase did not reach statistical significance, possibly due to the fact that the *Brca1* and *2* alleles are less efficiently rearranged compared to *p53* and *TgK18GT_{121}* alleles (Suppl. Fig. S3A-C). While it is possible that the deletion is inefficient, no progression was observed in $TgK18GT_{121}{}^{tg/+}/Brca1^{fl/fl}$ compared to $TgK18GT_{121}{}^{tg/+}$ mice up to nearly 2 years pi indicating that no deleted cells contributed to the tumor progression.

Induced $TgK18GT_{121}{}^{tg/+}/p53^{R172H/+}$, $TgK18GT_{121}{}^{tg/+}/Brca1^{fl/fl}/p53^{R172H/+}$ and $TgK18GT_{121}{}^{tg/+}/Brca2^{fl/fl}/p53^{R172H/+}$ mice carrying one mutant $p53^{R172H}$ allele developed mainly low grade SEOC at a frequency between 21% and 42% (Table 1, Fig. 2C, D). In contrast, compound mutant mice containing biallelic p53 modification (either $p53^{R172H/fl}$ or $p53^{fl/fl}$) presented with SEOC of all stages at an increased frequency of 68% to 88%, respectively (Table 1, Fig. 2E) indicating that biallelic p53 perturbation is associated with SEOC disease progression.

Consistent with other studies, mutant P53^{R172H} was not stably expressed in normal OSE or carcinoma cells from induced $TgK18GT_{121}{}^{tg/+}/p53^{R172H/+}$ mice as determined by IHC (Suppl. Fig. S4A). However, strong P53 expression was detectable in SEOC from $TgK18GT_{121}{}^{tg/+}/p53^{R172H/fl}$ mice indicating that an additional event interfering with the remaining p53 wild type allele is required for protein stabilization (Suppl. Fig. S4B, C). Interestingly, in 1 of 12 $TgK18GT_{121}{}^{tg/+}/p53^{R172H/+}$ and 2 of 19 $TgK18GT_{121}{}^{tg/+}/Brca1^{fl/fl}/$ $p53^{R172H/+}$ mice with stage III or IV SEOC (Table 1), tumor sections revealed small foci containing carcinoma cells with strong nuclear P53 expression suggesting spontaneous protein stabilization (Suppl. Fig. S4B). Microdissection and sequence analysis confirmed the loss of the p53 wildtype allele in tumor foci with increased nuclear P53 expression (Suppl. Fig. S4D).

Taken together, these data suggest that RB-TS and p53 cooperate in the development of metastatic SEOC. While only RB-TS inactivation is sufficient to initiate tumorigenesis, the mutation/loss of both *p53* alleles is required for the metastatic phenotype (stage IV disease).

Gene expression analysis of mouse ovarian tumors comfirms similarity to human SEOC

To determine whether $TgK18GT_{121}$, *p53, Brca1/2* driven tumors resemble human SEOC at the molecular level, we performed global gene expression analysis on 27 ovarian carcinomas and 3 pooled normal OSE samples (Supplementary Materials and Methods). Principle component analysis (PCA) and unsupervised hierarchical clustering revealed that the profiles of tumor samples were clearly distinct from normal OSE (Suppl. Fig. S5A). There was no obvious subclustering based on Brca1 or Brca2 status at the global gene expression level (Suppl. Fig. S5B) indicating that the majority of transcriptional changes are due to RB-TS and p53 pathway perturbation. Sample-level-enrichment-based pathway ranking (SLEPR) analysis (36) using Biocarta terms identified commonly altered pathways in tumors compared to normal samples (Fig. 5A). As expected, RB, p53, DNA damage signaling and repair pathway alterations were significantly changed in the majority of tumor samples (Fig. 5A, Suppl. Fig. S5C). To determine whether these changes reflect networks frequently disturbed in human high grade SEOC, TCGA curated pathways (6) were compiled and reproduced using mouse orthologous genes. As in the majority of human samples, the FOXM1 transcription factor network and its proliferation-related target genes were consistantly overexpressed in the murine tumors (Suppl. Fig S5C).

The comparison of four histological types of human ovarian cancer (serous, endometrioid, mucinous and clear cell) (10) with murine carcinoma samples revealed overlap of the murine and human SEOC samples in the space of the three top principal components relative to samples of other subtypes, indicating the strong similarity between these expression profiles (Fig. 5B). Additionally, cluster analysis of merged mouse and human data using classifier gene sets showed that mouse samples represent all 4 subgroups of human SEOC originally derived from the TCGA study (6): differentiated (40%, 11/27), immunoreactive (30%, 8/27), proliferative (15%, 4/27) and mesenchymal (15%, 4/27) (Fig. 5C) and are genetically distinct from diffuse malignant peritoneal mesotheliomas (Fig. 5D, Suppl. Fig. S5D) (37).

Metabolic changes in blood from mouse SEOC resemble changes seen in human ovarian cancer

To determine whether these mouse models can be utilized for biomarker discovery, we performed metabolomic profiling on blood from 15 controls and 15 compound mutants with either Brca1 or Brca2 deletion (Supplementary Materials and Methods) at three time points: prior to intrabursal injection (T0), after onset of disease in compound mutants (T1: 12-20 weeks pi), and at termination of the experiment (T2: 24-45 weeks pi) (Fig. 6A). At 12 to 20

weeks pi the OSE lesions in mice ranged from hyperplasia to early carcinoma (Stage IA), which had further progressed to advanced disease stages at the terminal time point (Supplementary Materials and Methods). Wild type mice had no significant changes in the OSE at any time point. Representative MRI scans of the ovaries are depicted in Fig. 6B.

A total of 318 named biochemicals were identified comprising all major biochemical groups. Two-way ANOVA identified biochemicals that had a significant main effect ($p <$ 0.05) for either genotype or time, with the greatest changes occurring at the terminal time point (Suppl. Fig. S6). Several metabolomic changes in tumor bearing animals overlap with previous findings obtained from tissue of human patients with metastatic ovarian cancer (38). These included increases in 2-hydroxybutyrate, three-hydroxybutyrate, citrate, α-tocopherol and short chain acyl carnitines as well as a decrease in taurine (Fig. 6C).

In addition, blood of animals bearing metastatic ovarian cancer contained decreased citrulline and increased spermidine and putrescine. The systemic redirection of ornithine from the urea cycle to polyamine biosynthesis was expected to result in a significant nitrogen stress to the animal and additional metabolites support this assertion. Specifically, the TCA cycle associated amino acids aspartate and glutamate were both increased in the blood of animals with metastatic ovarian cancer with aspartate increasing dramatically. Besides its role in the urea cycle, aspartate serves as the predominant backbone of pyrimidines in their de novo biosynthesis. The increased blood aspartate occurred simultaneously with increased abundance of many pyrimidine pathway metabolites, including orotate, uridine, thymidine and 2′-deoxycytidine (Fig. 6D, E). Several of the metabolites revealed temporal changes during disease progression (Fig. 6F) indicating that these mouse models provide a useful platform for the identification of candidate biomarkers for earlier detection and/or for monitoring treatment response.

Discussion

Here we report highly penetrant GEM models for epithelial ovarian cancer. By interfering with various combinations of RB, p53 and/or Brca protein functions, we dissected the relative contribution of these pathways to the development of stage IV disease. As in humans, mice developed peritoneal carcinomatosis, ascites and distant metastases. The histological morphology and immunophenotypical expression of markers, such as CA125, WT1, ER, PR mimics human SEOC. Additionally, transcriptional and metabolomic profiling confirmed that *Rb, p53, Brca1/2*-triple mutant tumors align with human SEOC and represent all 4 subclasses.

Previous studies showed that concomitant inactivation of Brca1 and p53 or Rb1 and p53 in mouse OSE cells can give rise to advanced ovarian carcinomas with serous histology (11, 14, 16). While one study showed that intrabursal inactivation of *Brca1* alone resulted in an increase in the number of preneoplastic changes in the OSE 240 days pi (39), in our models neither deletion/mutation of *p53, Brca1* or *Brca2* alone nor the combination thereof was sufficient to cause any significant histological changes in the surface epithelium, which is consistent with other reports (11, 13, 15, 16).

These data demonstrate that, of Brca1/2, p53 and RB pathway perturbation, only the latter was sufficient to *acutely* initiate disease. The fact that *Rb* deletion by itself did not result in histopathological abnormalities in previous studies (11, 13) implies that RB family members compensate for the loss of pRB. Indeed, loss of p130 in addition to Rb deficiency previously resulted in the acceleration of tumorigenesis in mouse models of lung adenocarcinoma and small cell lung cancer (40, 41). While we do not propose that impaired Rb-pathway function is the *only* possible initiating event, the present study (along with the high frequency of Rb

pathway aberrations in human SEOC) suggests that this is a common initiation, while impaired Brca1 or Brca2 and p53 facilitate SEOC progression.

The approach of targeting RB-TS inactivation specifically to epithelial cells via CK18 transcriptional regulation enabled us to minimize the appearance of ectopic tumors such as lymphomas and sarcomas. Lymphatic, mesenchymal and smooth muscle cells can be transformed more readily than epithelial cells, as seen in previous studies where conditional inactivation of *Brca1, p53* and *Rb* by intrabursal injection of Adeno-Cre resulted in the development of leiomyosarcomas due to transformation of smooth muscle cells in the ovarian bursa adjacent to the surface epithelium (13).

Mortality in SEOC patients is frequently due to the effects of disseminated abdominal disease on vital organs such as the gastrointestinal tract, and is secondary to distant metastasis. The latter may be present at the time of diagnosis (stage IV disease) or can arise following relapse. The GEM models described here not only recapitulate intraperitoneal spreading from a primary ovarian tumor but also the most common sites of distant metastases found in humans: pleura, lung and liver (27). Human ovarian tumors harboring mutations in both *p53* alleles were more likely associated with high grade SEOC, lymph node metastasis and the development of distant metastasis (42). In agreement with these data, the progression to stage III/IV SEOC pathology in the GEM models was dependent on biallelic mutation/inactivation of *p53*. While there was no obvious difference between complete loss or stabilization of mutant p53, future studies will explore whether any difference in ethiology or response to therapy results from these two mechanisms.

The combination of Brca1 inactivation with an initiation event did not appear to drive progression beyond stage I disease (non-invasive carcinoma). However, in combination with p53 aberration Brca1 inactivation may increase the incidence of disease. These findings are consistent with studies of Brca1, Brca2, and Li-Fraumeni families (43), showing that mutation carriers are predisposed to cancers, but the statistics of onset imply the need for stochastic initiating event(s). Future studies examining global genome and expression profiles of Brca wildtype and mutant SEOC may indicate potential differences. In addition, these tumors may respond differently to therapeutic agents. The models described here can be used to develop cell lines and allograft models for evaluating drug potency relative to Brca mutation status.

Although the exact cellular origin(s) of SEOC in humans is unclear, the emerging hypothesis is that the fallopian tube is the likely source (44, 45). This idea is based largely on early tubal lesions detected after prophylactic surgery in BRCA1 mutation carriers (46-49). Because progression cannot be followed in these cases, it is difficult to conclude that the lesions detected will give rise to SEOC. It is also possible that SEOC can arise from multiple sites. Experimental transformation of human OSE as well as human epithelial cells derived from the fallopian tube gave rise to high grade SEOC, respectively (32, 50). In this study, we showed that GEM-SEOC *can* initiate in the OSE, based on assessment of a significant number of induced mice at distinct times during progression in which disease was limited to the ovary. In some other cases, viral leakage to the adjacent oviduct (fallopian tube), was detected, but resulted in distinct pathology. Though the vast majority of human SEOC express Pax8, which is consistent with their origin in fallopian tube epithelium, it has not yet been shown to be a defining/requisite feature of these tumors. The preponderance of the remaining evidence (morphology, other IHC markers, and gene expression profiling) suggests that the murine tumors in our study resemble SEOC rather than mesotheliomas. Many of the existing murine ovarian carcinoma models have been derived by transformation of OSE (10, 11, 16). While one study showed similarity to human endometrioid ovarian cancer based on transcriptional profiling (10), SEOC-like mouse models were characterized

mainly based on histopathological features (11, 16). The status of Pax8 expression in these models was not described. Future experiments limiting induction to tubal epithelia in these models will facilitate addressing the cell or origin paradigm.

In conclusion, we have developed GEM models of SEOC with several key histopathological, immunophenotypical and genetic features of human SEOC. These models will serve as a foundation for future preclinical research.

Supplementary Material

Refer to Web version on PubMed Central for supplementary material.

Acknowledgments

References

1. Jemal A, Siegel R, Xu J, Ward E. Cancer statistics, 2010. CA: a cancer journal for clinicians. 2010; 60:277–300. [PubMed: 20610543]

2. Miller DS, Blessing JA, Krasner CN, Mannel RS, Hanjani P, Pearl ML, et al. Phase II evaluation of pemetrexed in the treatment of recurrent or persistent platinum-resistant ovarian or primary peritoneal carcinoma: a study of the Gynecologic Oncology Group. J Clin Oncol. 2009; 27:2686–91. [PubMed: 19332726]

3. Jemal A, Murray T, Ward E, Samuels A, Tiwari RC, Ghafoor A, et al. Cancer statistics, 2005. CA: a cancer journal for clinicians. 2005; 55:10–30. [PubMed: 15661684]

4. Neesham D. Ovarian cancer screening. Aust Fam Physician. 2007; 36:126–8. [PubMed: 17339973]

5. Cesario S. Advances in the early detection of ovarian cancer: How to hear the whispers early. Nurs Womens Health. 14:222–34. [PubMed: 20579298]

6. The Cancer Genome Atlas Research Network. Integrated genomic analyses of ovarian carcinoma. Nature. 2011; 474:609–15. [PubMed: 21720365]

7. Van Dyke T, Jacks T. Cancer modeling in the modern era: progress and challenges. Cell. 2002; 108:135–44. [PubMed: 11832204]

8. Sharpless NE, Depinho RA. The mighty mouse: genetically engineered mouse models in cancer drug development. Nat Rev Drug Discov. 2006; 5:741–54. [PubMed: 16915232]

9. Olive KP, Tuveson DA. The use of targeted mouse models for preclinical testing of novel cancer therapeutics. Clinical cancer research: an official journal of the American Association for Cancer Research. 2006; 12:5277–87. [PubMed: 17000660]

10. Wu R, Hendrix-Lucas N, Kuick R, Zhai Y, Schwartz DR, Akyol A, et al. Mouse model of human ovarian endometrioid adenocarcinoma based on somatic defects in the Wnt/beta-catenin and PI3K/Pten signaling pathways. Cancer Cell. 2007; 11:321–33. [PubMed: 17418409]

11. Flesken-Nikitin A, Choi KC, Eng JP, Shmidt EN, Nikitin AY. Induction of carcinogenesis by concurrent inactivation of p53 and Rb1 in the mouse ovarian surface epithelium. Cancer Res. 2003; 63:3459–63. [PubMed: 12839925]

12. Quinn BA, Xiao F, Bickel L, Martin L, Hua X, Klein-Szanto A, et al. Development of a syngeneic mouse model of epithelial ovarian cancer. J Ovarian Res. 2010; 3:24. [PubMed: 20958993]

13. Clark-Knowles KV, Senterman MK, Collins O, Vanderhyden BC. Conditional inactivation of Brca1, p53 and Rb in mouse ovaries results in the development of leiomyosarcomas. PLoS One. 2009; 4:e8534. [PubMed: 20046869]

14. Connolly DC, Bao R, Nikitin AY, Stephens KC, Poole TW, Hua X, et al. Female mice chimeric for expression of the simian virus 40 TAg under control of the MISIIR promoter develop epithelial ovarian cancer. Cancer Res. 2003; 63:1389–97. [PubMed: 12649204]

15. Quinn BA, Brake T, Hua X, Baxter-Jones K, Litwin S, Ellenson LH, et al. Induction of ovarian leiomyosarcomas in mice by conditional inactivation of Brca1 and p53. PLoS One. 2009; 4:e8404. [PubMed: 20046879]

16. Xing D, Orsulic S. A mouse model for the molecular characterization of brca1-associated ovarian carcinoma. Cancer Res. 2006; 66:8949–53. [PubMed: 16982732]

17. Song Y, Yang C, Pan W, Fathalizadeh A, Lu L, Gilbert D, et al. Conditional Initiation of Cancer in cytokeratin 18 or 19 Epithelial Cells in Genetically Engineered Mouse Strains. manuscript in preparation.

18. Integrated genomic analyses of ovarian carcinoma. Nature. 2011; 474:609–15. [PubMed: 21720365]

19. Stubdal H, Zalvide J, Campbell KS, Schweitzer C, Roberts TM, DeCaprio JA. Inactivation of pRB-related proteins p130 and p107 mediated by the J domain of simian virus 40 large T antigen. Mol Cell Biol. 1997; 17:4979–90. [PubMed: 9271376]

20. Sage J, Mulligan GJ, Attardi LD, Miller A, Chen S, Williams B, et al. Targeted disruption of the three Rb-related genes leads to loss of G(1) control and immortalization. Genes Dev. 2000; 14:3037–50. [PubMed: 11114892]

21. Simin K, Hill R, Song Y, Zhang Q, Bash R, Cardiff RD, et al. Deciphering cancer complexities in genetically engineered mice. Cold Spring Harb Symp Quant Biol. 2005; 70:283–90. [PubMed: 16869764]

22. Lozano G. The oncogenic roles of p53 mutants in mouse models. Curr Opin Genet Dev. 2007; 17:66–70. [PubMed: 17208429]

23. Jackson EL, Olive KP, Tuveson DA, Bronson R, Crowley D, Brown M, et al. The differential effects of mutant p53 alleles on advanced murine lung cancer. Cancer Res. 2005; 65:10280–8. [PubMed: 16288016]

24. Feki A, Irminger-Finger I. Mutational spectrum of p53 mutations in primary breast and ovarian tumors. Crit Rev Oncol Hematol. 2004; 52:103–16. [PubMed: 15501075]

25. Donehower LA, Harvey M, Vogel H, McArthur MJ, Montgomery CA Jr. Park SH, et al. Effects of genetic background on tumorigenesis in p53-deficient mice. Mol Carcinog. 1995; 14:16–22. [PubMed: 7546219]

26. Soslow, RA. Diagnostic Pathology of Ovarian Tumors. Springer; 2011.

27. Cormio G, Rossi C, Cazzolla A, Resta L, Loverro G, Greco P, et al. Distant metastases in ovarian carcinoma. Int J Gynecol Cancer. 2003; 13:125–9. [PubMed: 12657111]

28. Goldstein NS, Bassi D, Uzieblo A. WT1 is an integral component of an antibody panel to distinguish pancreaticobiliary and some ovarian epithelial neoplasms. Am J Clin Pathol. 2001; 116:246–52. [PubMed: 11488072]

29. Hwang H, Quenneville L, Yaziji H, Gown AM. Wilms tumor gene product: sensitive and contextually specific marker of serous carcinomas of ovarian surface epithelial origin. Appl Immunohistochem Mol Morphol. 2004; 12:122–6. [PubMed: 15354736]

30. Ordonez NG. Role of immunohistochemistry in distinguishing epithelial peritoneal mesotheliomas from peritoneal and ovarian serous carcinomas. The American journal of surgical pathology. 1998; 22:1203–14. [PubMed: 9777982]

31. Laury AR, Hornick JL, Perets R, Krane JF, Corson J, Drapkin R, et al. PAX8 reliably distinguishes ovarian serous tumors from malignant mesothelioma. Am J Surg Pathol. 2010; 34:627–35. [PubMed: 20414098]

32. Zheng J, Mercado-Uribe I, Rosen DG, Chang B, Liu P, Yang G, et al. Induction of papillary carcinoma in human ovarian surface epithelial cells using combined genetic elements and peritoneal microenvironment. Cell Cycle. 2010; 9:140–6. [PubMed: 20016289]

33. Nofech-Mozes S, Khalifa MA, Ismiil N, Saad RS, Hanna WM, Covens A, et al. Immunophenotyping of serous carcinoma of the female genital tract. Modern pathology: an official journal of the United States and Canadian Academy of Pathology, Inc. 2008; 21:1147–55.

34. Comin CE, Saieva C, Messerini L. h-caldesmon, calretinin, estrogen receptor, and Ber-EP4: a useful combination of immunohistochemical markers for differentiating epithelioid peritoneal mesothelioma from serous papillary carcinoma of the ovary. The American journal of surgical pathology. 2007; 31:1139–48. [PubMed: 17667535]

35. Barnetson RJ, Burnett RA, Downie I, Harper CM, Roberts F. Immunohistochemical analysis of peritoneal mesothelioma and primary and secondary serous carcinoma of the peritoneum: antibodies to estrogen and progesterone receptors are useful. American journal of clinical pathology. 2006; 125:67–76. [PubMed: 16482993]

36. Yi M, Stephens RM. SLEPR: a sample-level enrichment-based pathway ranking method -- seeking biological themes through pathway-level consistency. PLoS One. 2008; 3:e3288. [PubMed: 18818771]

37. Davidson B, Zhang Z, Kleinberg L, Li M, Florenes VA, Wang TL, et al. Gene expression signatures differentiate ovarian/peritoneal serous carcinoma from diffuse malignant peritoneal mesothelioma. Clinical cancer research: an official journal of the American Association for Cancer Research. 2006; 12:5944–50. [PubMed: 17062665]

38. Fong MY, McDunn J, Kakar SS. Identification of metabolites in the normal ovary and their transformation in primary and metastatic ovarian cancer. PLoS One. 6:e19963. [PubMed: 21625518]

39. Clark-Knowles KV, Garson K, Jonkers J, Vanderhyden BC. Conditional inactivation of Brca1 in the mouse ovarian surface epithelium results in an increase in preneoplastic changes. Exp Cell Res. 2007; 313:133–45. [PubMed: 17070800]

40. Ho VM, Schaffer BE, Karnezis AN, Park KS, Sage J. The retinoblastoma gene Rb and its family member p130 suppress lung adenocarcinoma induced by oncogenic K-Ras. Oncogene. 2009; 28:1393–9. [PubMed: 19151761]

41. Schaffer BE, Park KS, Yiu G, Conklin JF, Lin C, Burkhart DL, et al. Loss of p130 accelerates tumor development in a mouse model for human small-cell lung carcinoma. Cancer Res. 2010; 70:3877–83. [PubMed: 20406986]

42. Sood AK, Sorosky JI, Dolan M, Anderson B, Buller RE. Distant metastases in ovarian cancer: association with p53 mutations. Clin Cancer Res. 1999; 5:2485–90. [PubMed: 10499623]

43. Antoniou A, Pharoah PD, Narod S, Risch HA, Eyfjord JE, Hopper JL, et al. Average risks of breast and ovarian cancer associated with BRCA1 or BRCA2 mutations detected in case Series unselected for family history: a combined analysis of 22 studies. Am J Hum Genet. 2003; 72:1117–30. [PubMed: 12677558]

44. Karst AM, Drapkin R. Ovarian cancer pathogenesis: a model in evolution. J Oncol. 2010; 2010:932371. [PubMed: 19746182]

45. Przybycin CGKR, Ronnett BM, Shih IeM, Vang R. Are all pelvic (nonuterine) serous carcinomas of tubal origin? American Journal of Surgical Pathology. 2010; 34:1407–16. [PubMed: 20861711]

46. Rabban JT, Krasik E, Chen LM, Powell CB, Crawford B, Zaloudek CJ. Multistep level sections to detect occult fallopian tube carcinoma in risk-reducing salpingo-oophorectomies from women with BRCA mutations: implications for defining an optimal specimen dissection protocol. The American journal of surgical pathology. 2009; 33:1878–85. [PubMed: 19898224]

47. Finch A, Beiner M, Lubinski J, Lynch HT, Moller P, Rosen B, et al. Salpingo-oophorectomy and the risk of ovarian, fallopian tube, and peritoneal cancers in women with a BRCA1 or BRCA2 Mutation. Jama. 2006; 296:185–92. [PubMed: 16835424]

48. Callahan MJ, Crum CP, Medeiros F, Kindelberger DW, Elvin JA, Garber JE, et al. Primary fallopian tube malignancies in BRCA-positive women undergoing surgery for ovarian cancer risk reduction. J Clin Oncol. 2007; 25:3985–90. [PubMed: 17761984]

49. Agoff SN, Mendelin JE, Grieco VS, Garcia RL. Unexpected gynecologic neoplasms in patients with proven or suspected BRCA-1 or -2 mutations: implications for gross examination, cytology, and clinical follow-up. The American journal of surgical pathology. 2002; 26:171–8. [PubMed: 11812938]

50. Karst AM, Levanon K, Drapkin R. Modeling high-grade serous ovarian carcinogenesis from the fallopian tube. Proceedings of the National Academy of Sciences of the United States of America. 2011; 108:7547–52. [PubMed: 21502498]
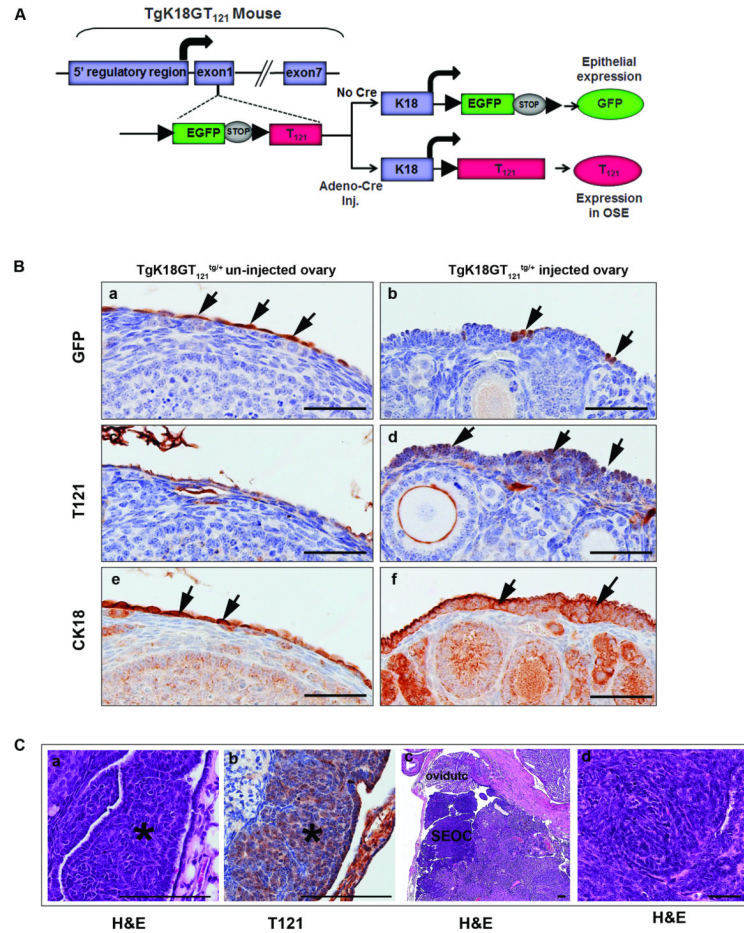
Figure 1.
Cre-mediated induction of genetic events in OSE cells by intra-bursal Adeno-Cre injection. A, Scheme depicting the targeting strategy. B, Expression of GFP, T121 antigen and CK18 in serial sections from ovaries of a $TgK18GT_{121}^{tg/+}$ mouse 3 months pi. GFP expression (a, brown, arrows) and lack of T_{121} expression (c) in uninduced OSE. Occasional GFP staining (b, arrows) and T_{121} expression (d, brown, arrows) in the induced OSE. Note that the OSE is hyperplastic with increased numbers of tightly packed columnar cells. IHC staining for CK18 (brown) depicts epithelial cells (e, f, arrows). C, CIS (*) in the induced OSE of a $TgK18GT_{121}^{tg/+}$ mouse 6 months pi (a). IHC confirming the expression of T_{121} (b; brown). SEOC with minimal invasion into underlying ovary in a $TgK18GT_{121}^{tg/+}$ mouse 24 months pi (c). Note unaffected fimbriae and oviduct. Higher magnification of SEOC (d). Scale bars in B represent 50 μm and in C 100 μm.
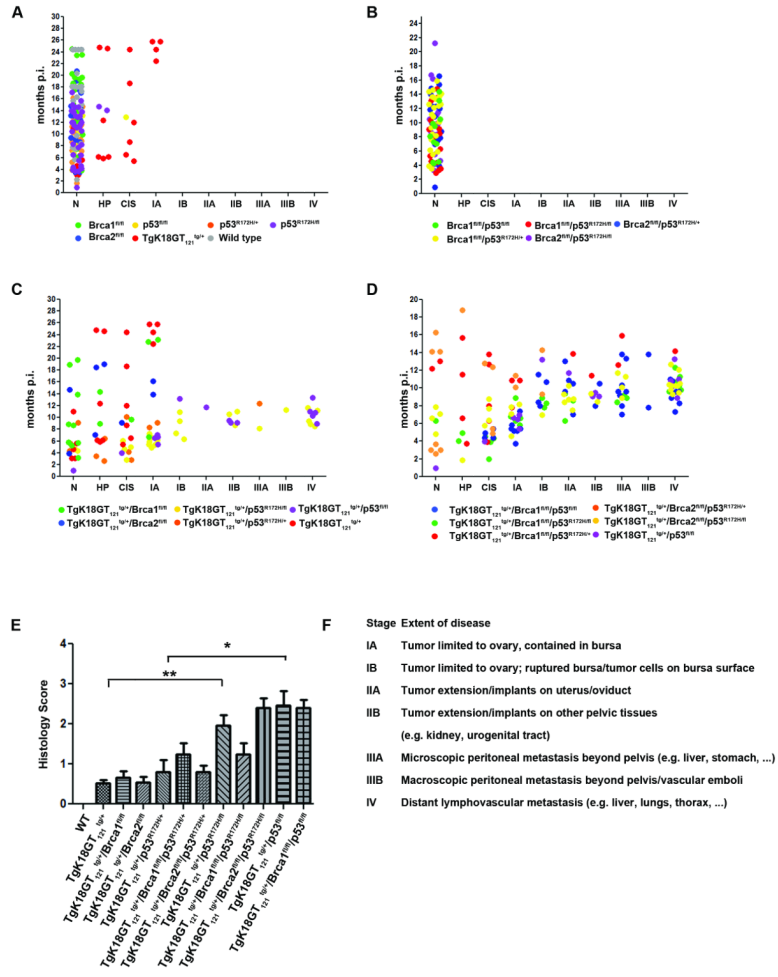
Figure 2.
Histopathological contribution of single and compound genetic events in the transformation of OSE. A, RB-TS pathway inactivation in $TgK18GT_{121}{}^{tg/+}$ mice is sufficient to initiate surface epithelial proliferation and early SEOC. B, Individual or combined inactivation of Brca1, Brca2 and/or p53 are insufficient to cause ovarian epithelial tumorigenesis. C, Combination of $TgK18GT_{121}$ and $p53$ alleles causes SEOC. D, Disease staging in mice with compound induction of RB-TS, p53 and Brca1 or Brca2. N: normal, HP: hyperplasia, CIS: carcinoma in situ. E, Statistical evaluation of disease progression based on histology score (HP=0.25, CIS=0.5, Stage IA=1.0, IB=1.5, IIA=2.0, IIB=2.5, IIIA=3.0, IIIB=3.5, IV=4). Mice removed from study before the age of 3 months were not included in the statistical analysis. Bars depict group mean histology score with error bars representing standard error of the means. One way-ANOVA with Bonferroni's Multiple Comparison post-test was used to test for significant differences between genotypes. F, Explanation of the histopathological staging system used. The classification was adopted from FIGO used in human ovarian carcinomas.
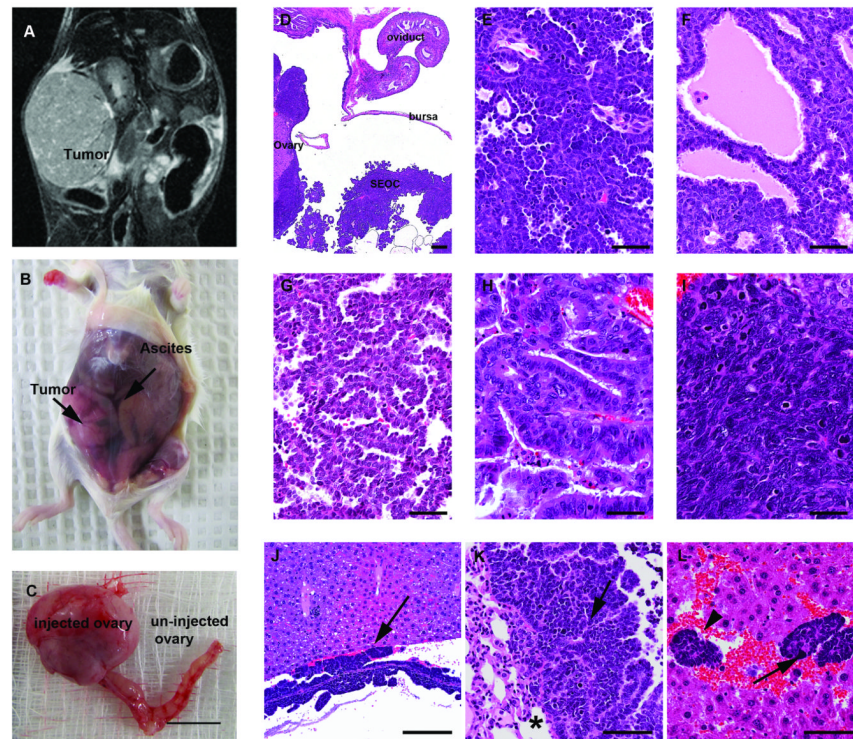
Figure 3.
Perturbation of Rb-TS, p53 and/or Brca1/2 in the OSE induces metastatic serous epithelial ovarian carcinomas. A, MRI of a $TgK18GT_{121}{}^{tg/+}/Brca1^{fl/fl}/p53^{R172H/fl}$ mouse showing a large ovarian tumor on the induced ovary. B, Abdominal distention and presence of ascites in the same mouse. C, Ovarian tumor and normal non-injected ovary of the same mouse 190 days pi. D, Early SEOC originating from the OSE (50×). Note intact bursa and unaffected oviduct. Range of different histological SEOC features: E, Papillary histology of SEOC shown in D; F, poorly differentiated glandular and microcystic histology; G, micropapillary/filigree; H, papillary and I, solid tumor histology. J, Intraperitoneal spreading (carcinomatosis) on serosal surface of liver (arrow). K, Pleural metastasis (arrow), note alveolar spaces in underlying lung parenchyma (*). L, Liver micrometastases showing the presence of papillary carcinoma within distended hepatic sinusoids (arrow and arrowhead). Scale bar in C represents 1 cm, in D to L 100μm.
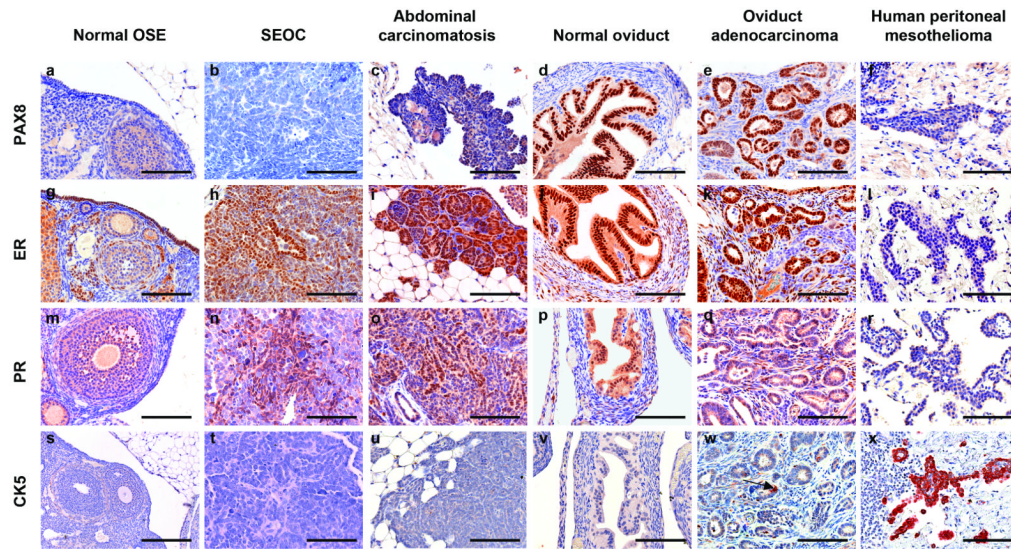
Figure 4.
Immunophenotype of SEOC arising from the mouse ovarian surface and oviduct epithelium, as well as abdominal carcinomatosis and human peritoneal mesothelioma. Normal mouse OSE (a, g, m s), carcinomas arising from the OSE (b, h, n, t), abdominal carcinomatosis (c, i, o, u), normal oviduct epithelium (d, j, p, v), adenocarcinomas arising from the oviduct (e, k, q, w) and human DMPM (f, l, r, x). Rare expression of CK5 indictated by arrow in w. Scale bars represent 200μm.

Figure 5.
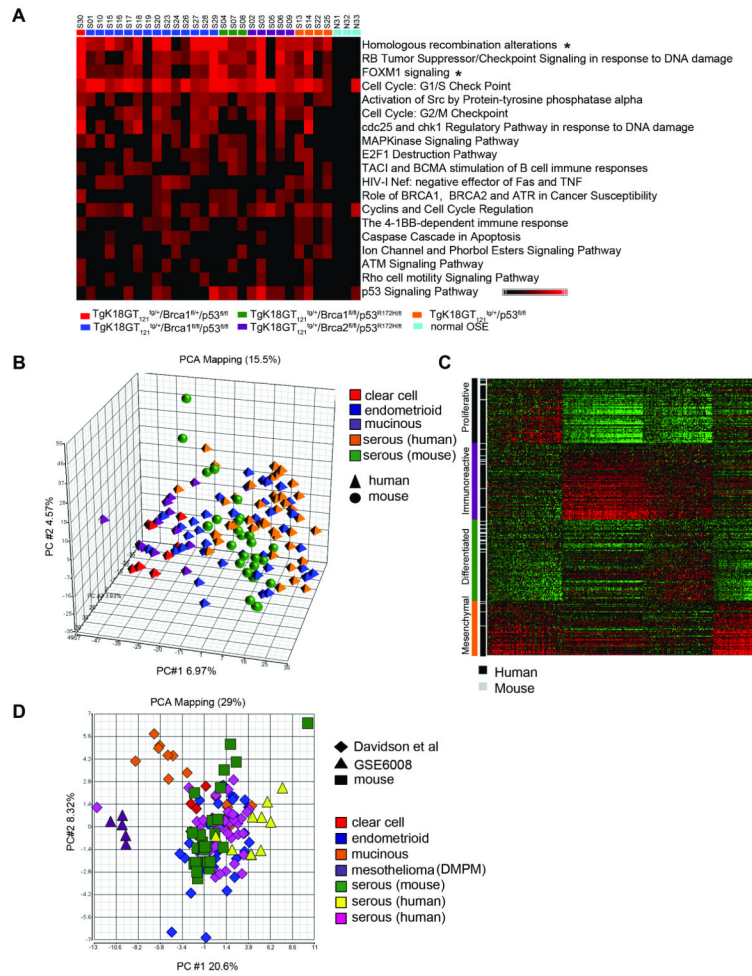Gene expression patterns and molecular subtypes of mouse SEOC mirror high grade human SEOC. A, Top ranked pathways enriched in tumors versus normals based on SLEPR analysis using Biocarta terms with inclusion of manually curated TCGA pathways (*). The enrichment scores were directly used to create the heatmap in ranked order (higher ranked genes at the top based on the permutated p-values of each pathway). Red, enriched significantly; black, no significant enrichment based on enrichment score of individual sample less than 1.3 ($p>0.05$) or Gene Hits less than 2. B, PCA of merged microarray data from mouse SEOC and four histological subtypes of human ovarian cancer [GSE6008; (10)]. C, Microarray data from mouse SEOC were merged and clustered together with human SEOC using the TCGA classifier genes (6). Genes in the heatmap were ordered based on their predictive classes of Differentiated, Immunoreactive, Mesenchymal and Proliferative tumor subtypes. The rows depict human (black) or mouse (grey) samples. The data in its original log2 intensity were scaled for purpose of display in heatmap: mean as 0 and standard deviation as 1 for each gene across all samples. D, PCA plot of the top two principal components for mouse tumors and a variety of subtypes of human ovarian carcinomas in the subset of the merged human-mouse array dataset containing the available human-mouse homologous genes out of 189-gene signature previously described to distinguish DMPM from SEOC (11).
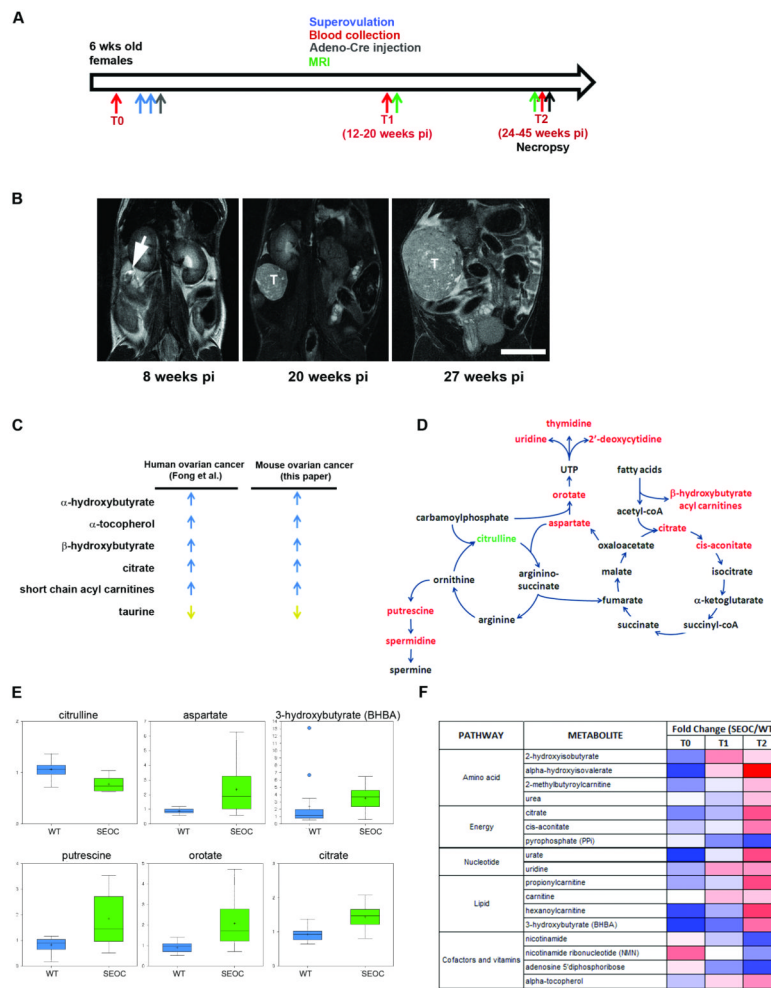
Figure 6.
Metabolomic profiling of blood during SEOC progression. A, Experimental design. B, Representative MRI scans from mice 8, 20 and 27 weeks pi, respectively. Arrow indicates the injected ovary, T indicates the ovarian tumor. Scale bar represents 1cm. C, Similar changes in human ovarian cancer tissue (38) and murine whole blood metabolome (this study). D, Integrative model of metabolomic changes observed in the blood of mice with SEOC compared to their littermate controls. Metabolites whose abundance increased are shown in red, decreased in green and unchanged or not detected in black. E, Boxplots comparing the abundance distribution of select metabolites between animals with metastatic ovarian cancer and their littermate (wt) controls at the terminal time points. F, Heat maps depicting temporal metabolite changes in SEOC compared to WT mice. The colors display each group mean level to the median for that compound, such that white represents the median, saturated red represents a two-fold increase relative to and saturated blue is one-half the median value.

Table 1

Histopathology of the ovarian surface epithelium and SEOC stages in Adeno-Cre injected mice.

Genotype	Normal (%)	Hyper-plasia (%)	Carcinoma in situ (%)	SEOC stages I-IV (%)	IA (%)	IB (%)	IIA(%)	IIB(%)	IIIA(%)	IIIB(%)	IV(%)	Other ovarian tumors (%)
Wild type	26/29 (90)	0/29 (0)	0/29 (0)	0/29 (0)	0/29 (0)	0/29 (0)	0/29 (0)	0/29 (0)	0/29 (0)	0/29 (0)	0/29 (0)	3/29 (10)
Brca1$^{fl/fl}$	19/19 (100)	0/19 (0)	0/19 (0)	0/19 (0)	0/19 (0)	0/19 (0)	0/19 (0)	0/19 (0)	0/19 (0)	0/19 (0)	0/19 (0)	0/19 (0)
Brca2$^{fl/fl}$	18/20 (90)	0/20 (0)	0/20 (5)	0/20 (0)	0/20 (0)	0/20 (0)	0/20 (0)	0/20 (0)	0/20 (0)	0/20 (0)	0/20 (0)	2/20 (10)
p53$^{R172H/+}$	23/26 (88)	0/26 (0)	0/26 (0)	0/26 (0)	0/26 (0)	0/26 (0)	0/26 (0)	0/26 (0)	0/26 (0)	0/26 (0)	0/26 (0)	3/26 (12)
p53$^{fl/fl}$	7/8 (78)	0/8 (0)	0/8 (0)	0/8 (0)	0/8 (0)	0/8 (0)	0/8 (0)	0/8 (0)	0/8 (0)	0/8 (0)	0/8 (0)	1/8 (11)
p53$^{R172H/fl}$	34/42 (81)	2/42 (5)	0/42 (0)	0/42 (0)	0/42 (0)	0/42 (0)	0/42 (0)	0/42 (0)	0/42 (0)	0/42 (0)	0/42 (0)	6/42 (14)
Brca1$^{fl/fl}$/p53$^{R172H/+}$	25/27 (93)	0/27 (0)	0/27 (0)	0/27 (0)	0/27 (0)	0/27 (0)	0/27 (0)	0/27 (0)	0/27 (0)	0/27 (0)	0/27 (0)	2/27 (7)
Brca1$^{fl/fl}$/p53$^{R172H/+}$	16/29 (55)	0/29 (0)	0/29 (0)	0/29 (0)	0/29 (0)	0/29 (0)	0/29 (0)	0/29 (0)	0/29 (0)	0/29 (0)	0/29 (0)	13/29 (45)
Brca1$^{fl/fl}$/p53$^{R173H/fl}$	8/21 (38)	0/21 (0)	0/21 (0)	0/21 (0)	0/21 (0)	0/21 (0)	0/21 (0)	0/21 (0)	0/21 (0)	0/21 (0)	0/21 (0)	13/21 (62)
Brca2$^{fl/fl}$/p53$^{R172H/+}$	17/20 (85)	0/20 (0)	0/20 (0)	0/20 (0)	0/20 (0)	0/20 (0)	0/20 (0)	0/20 (0)	0/20 (0)	0/20 (0)	0/20 (0)	2/20 (10)
Brca2$^{fl/fl}$/p53$^{R172H/fl}$	18/32 (56)	0/32 (0)	0/32 (0)	0/32 (0)	0/32 (0)	0/32 (0)	0/32 (0)	0/32 (0)	0/32 (0)	0/32 (0)	0/32 (0)	15/32 (47)
TgK18G$_{T121}$$^{tg/+}$	5/22 (23)	6/22 (27)	6/22 (27)	4/22 (18)	4/22 (18)	0/22 (0)	0/22 (0)	0/22 (0)	0/22 (0)	0/22 (0)	0/22 (0)	1/22 (5)
TgK18G$_{T121}$$^{tg/+}$/Brca1$^{fl/fl}$	9/15 (60)	2/15 (13)	1/15 (7)	3/15 (20)	3/15 (20)	0/15 (0)	0/15 (0)	0/15 (0)	0/15 (0)	0/15 (0)	0/15 (0)	0/15 (0)
TgK18G$_{T121}$$^{tg/+}$/Brca2$^{fl/fl}$	2/11 (18)	3/6 (11)	1/11 (9)	2/11 (18)	2/11 (18)	0/11 (0)	0/11 (0)	0/11 (0)	0/11 (0)	0/11 (0)	0/11 (0)	3/11 (27)
TgK18G$_{T121}$$^{tg/+}$/p53$^{R172H/+}$	3/12 (25)	3/12 (25)	3/12 (25)	3/12 (25)	2/12 (16)	0/12 (0)	0/12 (0)	0/12 (0)	1/12 (8)	0/12 (0)	0/12 (0)	0/11 (0)
TgK18G$_{T121}$$^{tg/+}$/Brca1$^{fl/fl}$/p53$^{fl/fl}$	2/19 (19)	4/19 (21)	5/19 (26)	8/19 (42)	3/19 (15)	0/19 (0)	1/19 (5)	1/19 (5)	2/19 (11)	0/19 (0)	1/19 (5)	0/19 (0)
TgK18G$_{T121}$$^{tg/+}$/Brca2$^{fl/fl}$/p53$^{R172H/+}$	7/19 (37)	1/19 (5)	4/19 (21)	4/19 (21)	2/19 (11)	2/19 (11)	1/19 (5)	0/19 (0)	0/19 (0)	0/19 (0)	0/19 (0)	3/19 (16)
TgK18G$_{T121}$$^{tg/+}$/p53$^{R172H/fl}$	2/29 (7)	0/29 (0)	4/29 (14)	21/29 (72)	7/29 (24)	4/29 (14)	0/29 (0)	3/29 (10)	1/29 (3)	1/29 (3)	5/29 (17)	2/29 (7)
TgK18G$_{T121}$$^{tg/+}$/Brca1$^{fl/fl}$/p53$^{R172H/fl}$	1/30(33)	2/30 (7)	4/30 (13)	21/30 (70)	5/30 (17)	3/30 (10)	3/30 (10)	0/30 (0)	2/30 (7)	1/30 (3)	7/30 (23)	2/30 (7)
TgK18G$_{T121}$$^{tg/+}$/Brca2$^{fl/fl}$/p53$^{R172H/fl}$	4/40 (10)	1/40 (3)	4/40 (10)	27/40 (68)	4/40 (10)	1/40 (3)	6/40 (15)	2/40 (5)	4/40 (10)	0/40 (0)	10/40 (25)	4/40 (10)
TgK18G$_{T121}$$^{tg/+}$/p53$^{fl/fl}$	1/17 (6)	0/17 (0)	1/17 (6)	15/17 (88)	4/17 (24)	2/17 (12)	1/17 (6)	0/17 (0)	3/17 (18)	0/17 (0)	5/17 (29)	0/17 (0)
TgK18G$_{T121}$$^{tg/+}$/Brca1$^{fl/fl}$/p5$^{fl/fl}$	1/50(2)	0/50 (0)	4/50 (8)	39/50 (78)	7/50 (14)	4/50 (8)	5/50 (10)	3/50 (6)	8/50 (16)	2/50 (4)	10/50 (20)	6/50 (12)